Research Article | Vol. 28, No. 22 / 26 October 2020 / Optics Express 32403
Optics EXPRESS

Octave-spanning mid-infrared femtosecond OPA in a $ZnGeP_2$ pumped by a 2.4 μm Cr:ZnSe chirped-pulse amplifier

SANG-HOON NAM,[1] VLADIMIR FEDOROV,[2] SERGEY MIROV,[2] AND KYUNG-HAN HONG[1,3,*]

[1]Research Laboratory of Electronics, Massachusetts Institute of Technology (MIT), Cambridge, MA 02139, USA
[2]Department of Physics, University of Alabama at Birmingham, Birmingham, AL 35294, USA
[3]MIT Lincoln Laboratory, Lexington, MA 02420, USA
*kyunghan@mit.edu

Abstract: We report on the highly efficient, octave-spanning mid-infrared (mid-IR) optical parametric amplification (OPA) in a $ZnGeP_2$ (ZGP) crystal, pumped by a 1 kHz, 2.4 μm, 250 fs Cr:ZnSe chirped-pulse amplifier. The full spectral coverage of 3–10 μm with the amplified signal and idler beams is demonstrated. The signal beam in the range of ~3 – 5 μm is produced by either white light generation (WLG) in YAG or optical parametric generation (OPG) in ZGP using the common 2.4 μm pump laser. We demonstrate the pump to signal and idler combined conversion efficiency of 23% and the pulse energy of up to 130 μJ with ~2 μJ OPG seeding, while we obtain the efficiency of 10% and the pulse energy of 55 μJ with ~0.2 μJ WLG seeding. The OPA output energy is limited by the available pump pulse energy (0.55 mJ at ZGP crystal) and therefore further energy scaling is feasible with multi-stage OPA and higher pump pulse energy. The autocorrelation measurements based on random quasi-phase matching show that the signal pulse durations are ~318 fs and ~330 fs with WLG and OPG seeding, respectively. In addition, we show the spectrally filtered 30 μJ OPA output at 4.15 μm suitable for seeding a Fe:ZnSe amplifier. Our ultrabroadband femtosecond mid-IR source is attractive for various applications, such as strong-field interactions, dielectric laser electron acceleration, molecular spectroscopy, and medical surgery.

1. Introduction

Femtosecond laser sources with an ultrabroadband spectral span in the mid-wave infrared (MWIR, 3–8 μm) and long-wave infrared (LWIR, 8–15 μm) portions of the mid-infrared (mid-IR) spectrum have interesting applications, ranging from molecular fingerprinting and studies of ultrafast dynamics [1,2] to strong-field laser sciences [3]. Besides the recently developed ultrafast CO_2 lasers at ~10 μm and Fe:ZnSe solid-state lasers at ~4 μm, parametric down-conversions, such as optical parametric amplification (OPA), optical parametric chirped-pulse amplification (OPCPA) and difference-frequency generation (DFG), are the commonly used method to generate high-energy ultrafast mid-IR laser pulses.

Ultrafast OPA with non-oxide nonlinear crystals, such as $ZnGeP_2$ (ZGP), $CdSiP_2$, and GaSe, pumped at ~2 μm wavelength, is found to be a promising way of accessing the full mid-IR range up to ~15 μm [4–7] due to their broad transparency range and favorable phase-matching conditions. Particularly, thanks to its high effective nonlinearity (77 pm/V) and high damage threshold, ZGP has been the most widely used for high-energy mid-IR OPA [4] and OPCPA systems [5]. Mid-IR ZGP OPA with a greater-than-octave-spanning spectral bandwidth was demonstrated using a ~30 fs, 2.1 μm OPCPA pump source [6], but the conversion efficiency was as low as 4% due to a relatively thin (0.5 mm) ZGP crystal. Picosecond ~2.05 μm Ho-doped lasers

#405648 https://doi.org/10.1364/OE.405648
Journal © 2020 Received 18 Aug 2020; revised 21 Sep 2020; accepted 30 Sep 2020; published 12 Oct 2020

Optics EXPRESS

are also suitable for pumping ZGP OPA/OPCPA [5,8], but relatively narrow mid-IR bandwidths have been obtained from those OPA/OPCPA systems. For achieving the broadest mid-IR phase matching bandwidth available from ZGP OPA/OPCPA, a slightly longer pump wavelength at ~2.5 μm is strongly suggested [4].

Transition-metal-doped II-VI materials, such as Cr:ZnSe, Cr:ZnS, and Fe:ZnSe, are found to be a suitable choice for direct lasing in the mid-IR with broad wavelength tunability and ultrashort pulse generation. These materials combine superb ultrafast laser capabilities with high nonlinearity of wide-bandgap zinc-blende semiconductors. For example, Cr:ZnSe and Cr:ZnS [9–17] support all standard regimes of femtosecond lasers and amplifiers at ~2.4 μm and also enable efficient frequency conversion of ultrashort pulses via $\chi^{(2)}$ and $\chi^{(3)}$ nonlinearity. They are emerging as excellent mid-IR lasing materials due to the improved crystalline growth and doping process [9–11]. In this regard, recently available mJ-level, femtosecond, ~2.4 μm Cr:ZnSe laser amplifiers [17,18] are an interesting source for pumping ZGP OPA as well as directly driving strong-field interactions [19]. Cr:ZnSe laser amplifiers can possibly establish themselves as an important laser source in the mid-IR range like CPA Ti:sapphire lasers in the near-IR range. For these reasons, robust and relatively compact, femtosecond mid-IR Cr:ZnSe lasers can get increasingly popular in ultrafast mid-IR research.

In this paper, we demonstrate a highly efficient, femtosecond ZGP OPA system fully covering the mid-IR range of 3–10 μm using a 2.4 μm Cr:ZnSe pump laser. We first describe the details of the pump laser and then compare the OPA phase matching conditions in ZGP between 2.4 and 2.05 μm pumping. In the experimental sections, we present a systematic study performed using two different methods for signal generation in the 3–5 μm range: white light generation (WLG) in YAG [19] and optical parametric generation (OPG) in ZGP [4]. We obtain the output energy of up to ~130 μJ and a conversion efficiency of ~23% from the OPG seeding. More detailed characterization of pulse energy, signal pulse duration, and beam profiles will be presented. Additionally, we demonstrate the spectrally filtered OPA at 4.15 μm, suitable for seeding a Fe:ZnSe amplifier. Our demonstration offers an energy scalable and technically simple platform of ultrafast laser sources with the possible coverage of the entire mid-IR region for investigating spectroscopic chemical detections and phase-sensitive strong-field interactions [1,6].

2. Cr:ZnSe pump laser at 2.4 μm

The Cr:ZnSe laser for pumping our ZGP OPA is a femtosecond, mid-IR chirped-pulse regenerative amplifier (CLPF-CPA, IPG Photonics) operating at a 1 kHz repetition rate, pumped by a Q-switched Ho:YLF laser. The Cr:ZnSe regenerative amplifier [18] is seeded by a Kerr-lens-mode-locked femtosecond Cr:ZnS laser oscillator. The Cr:ZnS oscillator and Ho:YLF pump are optically pumped by radiations of an Er-doped fiber and Tm-doped fiber lasers, respectively. The diagram of the Cr:ZnSe CPA laser is shown in Fig. 1(a). The main system, as indicated by the red arrows of the 2.4 μm beam, consists of two units: grating-based stretcher/compressor unit and amplifier unit. Stretched pulses are amplified in the Cr:ZnSe regenerative amplifier and then re-compressed in the compressor, which outputs amplified femtosecond pulses. The free-space optical paths are isolated from the environment. This system is cooled by water and purged by industrial nitrogen gas. The output spectrum has a center wavelength of 2.40 μm with the peak at 2.45 μm, as shown in Fig. 1(b). The spectral bandwidth is broader than 100 nm in full-width at half maximum (FWHM) supporting a transform-limited pulse duration of <200 fs. The measurement was carried out after ~1 hour of warm-up of the system. The oscillations in the spectroscopic signal are mostly attributed to the water vapor absorptions. The power stability measured at 1.23 W (or 1.23 mJ in energy) is better than 5% rms over 10 minutes, as shown in Fig. 1(c). This initial transient appears to be related to the humidity fluctuation of the regenerative amplifier cavity during the warm-up time. In the latter 5-minute range of the same graph, the shot-to-shot stability is as good as 2.5% rms, which can be further improved by reducing the

Optics EXPRESS

timing jitter of the Ho:YLF pump pulses. The average output power and the shot-to-shot stability do not degrade over an entire day (~8 working hours). The inset is the near-field output beam profile measured after the compressor. The beam profile is near Gaussian for both axes with some ellipticity of ~0.6. In Fig. 1(d), the pulse duration of ~250 fs was measured using intensity autocorrelation (AC) of output pulses.

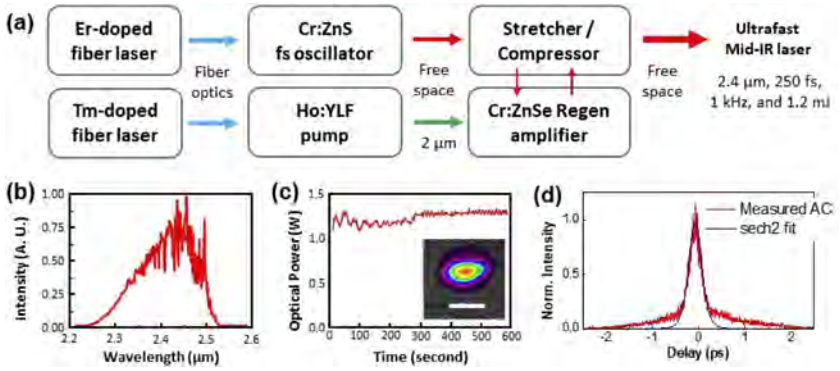

Fig. 1. (a) A femtosecond Cr:ZnSe CPA laser system, including: femtosecond Cr:ZnS oscillator; stretcher/compressor unit; Cr:ZnSe regenerative amplifier unit. The pump lasers include an Er-doped fiber laser for the Cr:ZnS oscillator, and a Tm-doped fiber and a Ho:YLF pump lasers for the Cr:ZnSe amplifier. The system is cooled by water and purged by N_2 gas. (b) Optical spectrum of compressed pulses, (c) Optical power (inset: output beam profile measured at 1 m distance from the output window, where the white line is a 8 mm scale bar corresponding to the horizontal beam diameter in $1/e^2$), and (d) Intensity AC of output pulses (red) with $sech^2$ function fitting (black) showing the pulse duration of ~250 fs in FWHM.

3. OPA setup and amplification results

3.1. Phase matching in ZGP for mid-IR OPA

We calculate the phase matching related parameters, such as angular tuning curve, effective nonlinear coefficient (d_{eff}), group velocity mismatch (GVM), and pulse splitting length, in ZGP pumped at 2.40 μm wavelength for broad mid-IR OPA, using the SNLO software [20] and Sellmeier equation [21]. These parameters are compared with the cases of 2.05 μm pump wavelength that are available with near-IR-pumped OPA/OPCPA systems [22] or Ho-doped lasers [23]. The angular tuning curves for type-I phase matching ($e_{pump} \rightarrow o_{signal} + o_{idler}$) corresponding to the broadest spectral range of the signal and idler beams are shown in Fig. 2(a). With the pump wavelength at 2.40 μm and θ=49.0°, ZGP gives perfect phase matching at around 3.2, 4.5, 5.6, and 9.5 μm while the good phase matching over the full band of 3 – 10 μm can be achieved within ~1° of angle at 49°. The additional band of pump spectrum along with the beam divergence helps to widen the amplified bandwidth and fill up the spectral gaps. In contrast, the 2.05 μm pump requires ~4° of angle tuning of ZGP to achieve the phase matching over 3 – 10 μm though it allows excellent phase matching for the range of 7 – 12 μm at θ = ~50.5°.

Figure 2(b) shows the d_{eff} value for two pump wavelengths. Changes in d_{eff} vary in the range of 3 – 12 μm by 1% for 2.40 μm and 5% for 2.05 μm, allowing for efficient amplification across the broad spectral range. Although the difference is not significant, the d_{eff} value at the phase matched angle for the 2.40 μm pump is higher in the 3 – 9 μm range. The GVM curves between pump and signal as well as pump and idler are shown in Fig. 2(c). Broad and flat regions of GVM are obtained with both 2.40 and 2.05 μm, but the ~2x smaller GVM values with 2.40 μm pump in the signal (~3 – 5 μm) and idler (~5 – 10 μm) are more favorable for broadband amplification

Optics EXPRESS

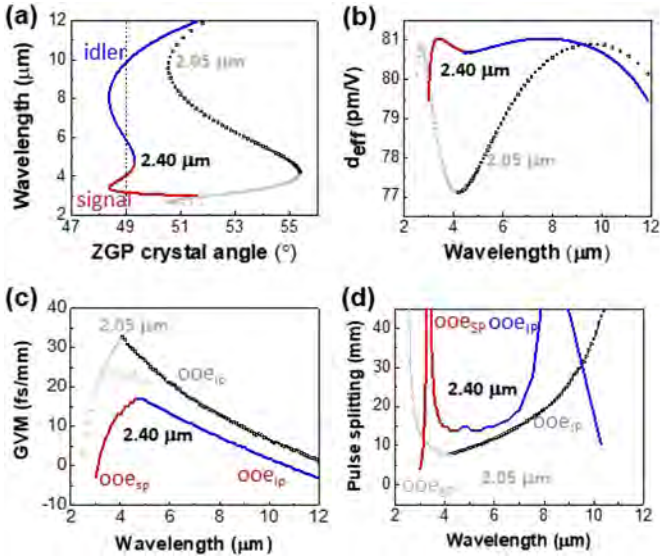

Fig. 2. Phase matching curves from SNLO: (a) Angle dependence, (b) Effective nonlinear coefficient, (c) Group velocity mismatch (GVM), and (d) Pulse splitting length for a type-I OPA in ZGP pumped by 250 fs, 2.40 and 2.05 μm pulses, respectively.

than with 2.05 μm pump. The interaction length over which parametric amplification occurs is expressed as the pulse splitting length [24,25], as shown in Fig. 2(d). The temporal walk-off between two pulses becomes the same as the pump pulse duration after the propagation over the pulse splitting length. Using the calculated GVM, the pulse splitting length has been derived with a pulse duration of 250 fs from the Cr:ZnSe CPA laser. The relatively long pulse splitting length allows for the reduction of the required pump intensity to achieve high gain in ZGP crystals, enabling the use of longer crystals for amplification. According to Fig. 2(d), with 2.40 μm pump the pulse splitting does not occur in up to ~13 mm of ZGP crystal over the entire 3 – 10 μm range, which is ~2x longer than that with the 2.05 μm pump. Based on this calculation and the commercial availability, a 5 mm-long ZGP crystal (BAE systems) is chosen for the experiment of broadband OPA free of pulse splitting although a ZGP crystal as long as ~13 mm could be used to increase the gain or lower the pump peak power. All the parameters plotted in Figs. 2(a)-(d) support that the 2.40 μm pump is more advantageous than 2.05 μm pump for broadband OPA in the range of 3 – 10 μm.

3.2. OPA setup

The experimental layout of the mid-IR ZGP OPA system is composed of the signal generation stage, the pump arm, and a single ZGP OPA stage, as illustrated in Fig. 3(a). The broadband mid-IR seed beam in the range of ~3 – 5 μm as OPA signal is generated in the $\chi^{(2)}$ or $\chi^{(3)}$ nonlinear crystal (NL in Fig. 3(a)) pumped by the common 2.4 μm Cr:ZnSe laser. In our experiment we use either WLG ($\chi^{(3)}$) based on laser filamentation in a YAG crystal or OPG ($\chi^{(2)}$) in a ZGP crystal. The 2.4 μm pump beam is split into the seed generation stage (reflection) and the OPA arm (transmission) using an uncoated ZnSe wedge. The ~100 μJ portion out of the 1.2 mJ, 2.4 μm pump is reflected off the wedge and used for the signal generation.

Optics EXPRESS

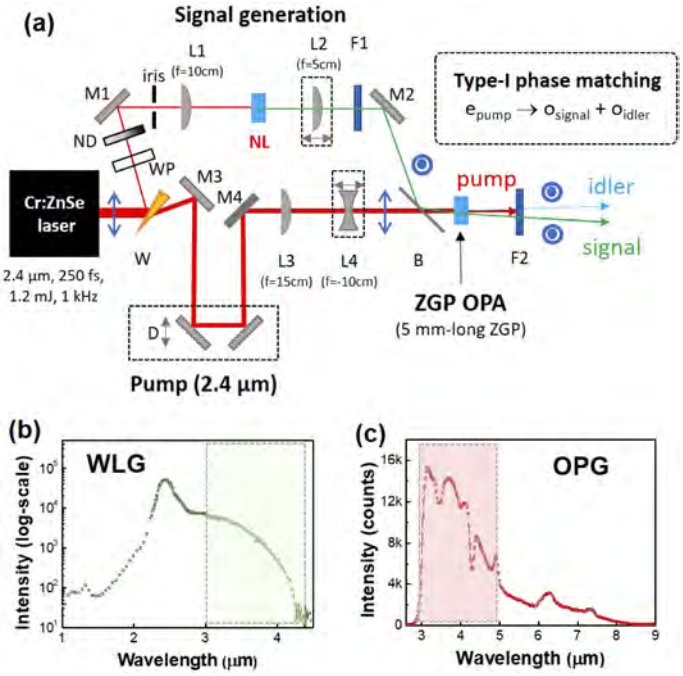

Fig. 3. (a) Experimental setup of mid-IR ZGP OPA. Red lines, 2.4 μm pump beam; green line, signal (seed) beam; blue dotted line, idler beam. M1-M4: Al mirrors; L1-L4: CaF_2 lenses; F1: 3 μm LPF; F2: 4.5 or 7 μm LPF; W: ZnSe wedge; D: delay stage; NL: nonlinear crystal (YAG or ZGP); B: 300-μm-thick Brewster Si plate; WP: λ/2 waveplate, (b) WLG spectrum in logarithmic scale, where the shaded area indicates the seed spectrum, and (c) OPG spectrum in linear scale, where the shade area indicates the seed spectrum.

3.2.1. Signal generation using WLG

The supercontinuum generation (SCG) process from a single laser filament in a solid is widely used for WLG covering multi-octave spectral bandwidth. The WLG seeding has also commonly been used for near-IR-pumped OPA systems. The OPA signal bandwidth of ~3 – 5 μm is relatively close to the pump wavelength of 2.4 μm and can be reached via WLG. In particular, since the SCG process can maintain the temporal coherence of the pump pulse, *i.e.*, the fixed phase relationship between pump and signal, the carrier-envelope phase (CEP) of idler pulse is passively stabilized in the OPA process due to the cancellation of the common phase offset of pump and signal pulses, which is very useful for driving phase-sensitive strong-field interactions in the few-cycle regime.

In our experiment, we utilize a 6 mm-long YAG crystal as filamentation medium for WLG. YAG is found to be suitable for mid-IR laser filamentation [26] due to the broad transmission range in the mid-IR, high damage threshold and moderately small, negative group-delay dispersion value of -149 fs^2/mm at ~2.4 μm suitable for soliton-like pulse propagation without significant pulse broadening. The optical layout of WLG is shown in the signal generation arm in Fig. 3(a). The polarization of the laser beam reflected off the wedge plate is changed to vertical using a half waveplate (WP) in order to later satisfy type-I phase matching at the OPA stage. The pulse energy and beam size are adjusted using a neutral density (ND) filter and an iris, respectively, so that we obtain the single-filament WLG. The input beam diameter of ~6 mm is found to be optimal when ~15 μJ pump beam is focused onto YAG using an f=10 cm CaF_2 lens (L1). The position of the YAG crystal relative to the beam focus is further optimized such that we maximize the mid-IR extension to ~4.5 μm while maintaining the single filament. The optimal crystal position

Optics EXPRESS

is found to be ~6 mm behind the focus, measured from the input surface of YAG crystal. The produced white-light beam is collimated with an f=5 cm CaF_2 lens (L2) and loosely focused at the OPA stage with ~3 mm in diameter.

The WLG spectrum is recorded using a fiber-coupled near-IR spectrometer (NIR-256-2.5, Ocean Optics Inc.) for the wavelength range of 1.0–2.5 μm and a scanning-grating monochromator (MicroHR, Horiba JY Inc.) with a liquid-nitrogen-cooled HgCdTe (MCT) detector for the mid-IR wavelength (2 – 12 μm). Figure 3(b) shows the measured spectrum that spans more than octave bandwidth in logarithmic scale from the near-IR to mid-IR, where the spectra from the two spectrometers are stitched at ~2.2 μm. The mid-IR spectral edge reaches ~4.5 μm although the CO_2 absorption at ~4.3 μm hinders the clear cutoff wavelength. For the purpose of OPA seeding, the residual 2.4 μm pump beam is removed by a long-pass filter (LPF) with the cut-on wavelength at 3.0 μm (EOC Inc.) and the pulse energy in the signal band (3.0 – 4.5 μm) is ~0.2 μJ.

3.2.2. Signal generation using OPG

The ultrabroadband phase matching and high d_{eff} value, as discussed in section 3.1, make the ZGP crystal very attractive for not only OPA but also OPG as another method of OPA signal (seed) generation when pumped at 2.4 μm of wavelength. For OPG we use a 5 mm-long, anti-reflection (AR)-coated ZGP crystal (θ = 49°, BAE systems) in a collinear type-I phase matching geometry. As shown in Fig. 3(a), we use the same focusing and recollimating optics as the WLG seeding setup for compatibility. The pump polarization is, however, unchanged unlike WLG as the OPG signal beam will have the orthogonal polarization. The pulse energy and beam size are adjusted using the same ND filter and iris to maximize OPG while avoiding any optical damage. With the input beam diameter of ~2 mm the pulse energy of ~25 μJ is used for pumping ZGP. The pump beam is focused into the ZGP crystal using the same f=10 cm CaF_2 lens and the ZGP crystal is located ~2 mm behind the focal position. The produced OPG signal and idler beams are collimated with the same f=5 cm CaF_2 lens and loosely focused at the OPA stage. The residual 2.4 μm pump beam is removed by the 3.0 μm LPF and the OPG spectrum is recorded using the same mid-IR spectrometer. We use two additional LPFs with the cut-on wavelengths at 4.5 and 7.3 μm (EOC Inc.), respectively, to analyze the signal and idler spectra by removing high-order diffractions. Figure 3(c) shows the obtained OPG spectrum, which is the combination of three measurements with three LPFs including the 3.0 μm LPF. The spectrum covers from 3.0 to 8.5 μm in the linear scale. The pulse energy in the signal range is ~2.3 μJ. The OPG itself has a conversion efficiency into the signal band of ~9% from the pump energy, which is found to be significantly more efficient than WLG. It should be noted that we have a random phase relationship between the pump and signal pulses in the OPG process. A minor contribution of OPG idler band to the OPA seeding may exist, but the OPA process is still dominated by the OPG signal band because the OPG idler beam is estimated to have nearly an-order-of-magnitude lower fluence than that of the signal beam at the OPA crystal due to the lower pulse energy and larger beam size.

3.2.3. ZGP OPA stage

The signal beam from either WLG or OPG is amplified in an AR-coated 5-mm-long ZGP crystal (θ = 49°, BAE) which is identical to the ZGP crystal for OPG. As shown in the pump arm of Fig. 3(a), the pump beam is delivered to the ZGP crystal after a delay stage and a telescope with two CaF_2 lenses with f=15 cm (L3) and -10 cm (L4), respectively. The telescope down-collimates the pump beam and allows the beam size adjustment at the ZGP crystal for maximizing the gain without inducing the optical damage and excessive superfluorescence (SF) which is essentially OPG competing with OPA in the presence of seeding. The vertically polarized pump and horizontally polarized signal beams are spatially combined at the ZGP crystal for the collinear type-I OPA with a 300 μm-thick Brewster-angle Si wafer that works as a polarizing beam splitter

Optics EXPRESS

(PBS) to transmit the pump beam while reflecting the signal beam. The pump beam with 0.55 mJ of energy is available for actually pumping the ZGP crystal due to the reflection loss at the metallic mirrors and transmission loss at the wedge plate, the lenses, and the silicon plate. Even though the OPA is basically achieved in a collinear geometry, we can induce ~2° angle between the pump and signal beams when we need to spatially separate the signal and idler beams.

3.3. Amplification results and discussion

3.3.1. Optimization of OPA

We first carried out the WLG-seeded OPA experiment and systematically optimized the OPA conditions. The optimization started with the pump beam because the pump beam intensity is the most critical to determine the OPA gain while not damaging the crystal. The pump energy was fixed at ~0.4 mJ and the pump beam size was adjusted using the telescope in Fig. 3(a), such that we start observing noticeable SF (>10 μJ) without the seed (signal) beam. This condition indicates the OPA gain must be high enough to be measured once the seed beam is spatially and temporally overlapped with the pump beam. Then we aligned the seed beam to the pump beam while letting the seed beam size (>3 mm in dia.) overfill the pump beam size to suppress SF generated from the unseeded part of the pump beam. Finally, the temporal overlap between the two beams was ensured using the delay stage. Once we observed the gain, we fine-tuned the spatial and temporal overlaps again. Figure 4(a) shows the typical amplified spectra from WLG-seeded OPA. The blue solid line represents the amplified spectrum of the signal, the green dashed line, the input WLG seed, and the red solid line, the SF without seeding. The WLG spectrum is plotted in linear scale unlike Fig. 3(b). It should be noted that SF in the presence of a seed is much weaker than SF without a seed because the seed takes over the gain from the noise. The signal gain was as high as $\sim 4 \times 10^2$. To find out the optimal pump beam size for OPA, we scanned the position of f=-10 cm lens in the telescope (L4 in Fig. 2(a)). Figure 3(c) indicates that the beam diameter of 2.0 – 2.2 mm at the ZGP crystal was optimal for obtaining high conversion efficiency while maintaining the minimal SF. The conversion efficiency itself is nearly flat at the beam diameter of 1.5 – 2.2 mm. The pump intensity at 2.0 mm of beam diameter is estimated to be ~35 GW/cm^2, which takes into account the ~30% of pulse energy in the temporal pedestal (Fig. 1(d)). The conversion efficiency started dropping as the beam diameter gets smaller than ~1.5 mm. An excessive pump intensity not only induces the strong SF but also can eventually cause a permanent surface/bulk damage.

We characterized the optical spectrum and beam profile of the WLG-seeded OPA output using the mid-IR spectrometer and a mid-IR beam profiler (WinCamD, DataRay), respectively, as shown by Fig. 4(c). For this measurement the pump pulse energy was increased to 0.55 mJ and the signal and idler combined, output pulse energy was 55 μJ. Despite the low seed energy of ~0.2 μJ in the signal band, the amplified spectrum fully covers the wavelength from 3 to 10 μm, confirming that the ~2.4 μm pump wavelength is crucial to obtain the octave-spanning phase matching band of ZGP in the mid-IR along with high gain, as discussed in section 3.1. The long-wavelength tail reaches up to ~12 μm, limited by the absorption band of ZGP, but the spectral contents beyond 10 μm was negligible with the unfavorable phase matching. As a result, we were able to generate more-than-octave-spanning continuum-like spectrum in the mid-IR from the single OPA source. The spectral peak at 2.4 μm is the residual pump beam after the 3 μm LPF. The wavelength range of 3.0 – 4.5 μm is considered as signal band while the 4.5 – 10 μm range, as idler band. Although ~4.8 μm is the nominal degenerate point of the center wavelength of pump beam, it is not sharply defined due to the broad spectral pump band of ~2.25 – 2.52 μm (Fig. 1(b)). The idler itself has an octave-spanning spectrum in full width at 10% maximum and can be compressed to ~1.5 optical cycles in duration with the passive CEP stability. The absorption line of atmospheric CO_2 at ~4.3 μm is clearly observed along with some other fine structures. A vacuum, noble-gas purging, or dry-air purging laser enclosure could be used to

Optics EXPRESS

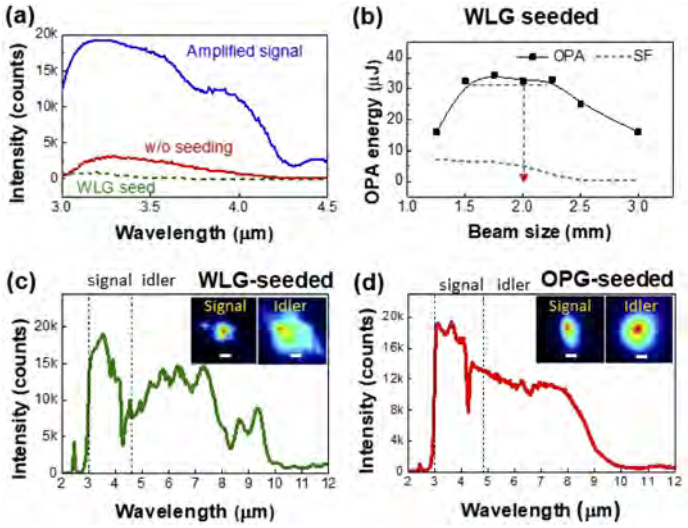

Fig. 4. Optimization and output spectra of OPA. (a) Optical spectra of WLG-seeded pulses. Blue solid line, amplified signal; green dotted line, WLG seed; red solid line, SF without seeding. (b) OPA (black solid line with squares) and SF (black dotted line) output energies versus beam size at the ZGP crystal. The red dotted line indicates the typical OPA operating point in this work. Output spectrum of the WLG-seeded OPA (c) and the OPG-seeded OPA (d), respectively, measured after a 3 μm LPF. The insets are the beam profiles of the signal and idler beams, where the white scale bars correspond to 2 mm in length.

remove these spectral features and to further increase the output pulse energy. The near-field beam measurements of both signal and idler (the inset of Fig. 4(c)) show decent beam profiles with a single peak and the idler beam size is much larger than the signal beam size, as expected from wavelength-dependent diffraction. Here, a 3.5 – 4.5 μm bandpass filter (BPF) was used for the signal beam and a 4.5 μm LPF, for the idler beam.

The same optimization process was applied to the OPG-seeded OPA. Due to much higher seed energy of ~2.3 μJ, the OPA output pulse energy (signal + idler) was enhanced to 130 μJ at 0.55 mJ pumping. The corresponding optical spectrum and the spatial beam profile are shown in Fig. 4(d). While the signal and idler combined spectrum covers the same range from 3 to 10 μm as the WLG-seeded case, the spectral contents are more evenly distributed due to the flatter seed spectrum from OPG (Fig. 3(d)). The near-field beam profiles were also found to be more uniform than the WLG-seeded OPA beams. Detailed comparison of performance between two OPA configurations will be discussed in next section.

3.3.2. Comparison of WLG-seeded and OPG-seeded OPA

We performed systematic studies of WLG-seeded OPA (WLG/OPA) and OPG-seeded OPA (OPG/OPA) using the same experimental setup of Fig. 3(a). The measurements of pulse energy and conversion efficiency vs. pump energy are shown in Figs. 5(a) and (b), respectively, where the 2.4 μm pump beam diameter at the ZGP crystal was set to ~2.0 mm. The slope of both OPA outputs vs. pump energy in Fig. 5(a) is almost linear, indicating that saturation or back-conversion is not noticeably high. The maximum output energy (signal + idler) was as high as 55 μJ from WLG/OPA and 130 μJ from OPG/OPA. The ~10 times higher seed energy from OPG is the obvious reason why we obtained much higher output energy from OPG/OPA. The corresponding conversion efficiencies were up to 10% and 23% for WLG/OPA and OPG/OPA, respectively. To the best of our knowledge, the conversion efficiency of 23% is the highest among the

Optics EXPRESS

octave-spanning or greater-than-octave-spanning OPA systems in the mid-IR. Considering the ~80% transmittance of the 3 μm LPF filter used for the energy measurement, we even estimate ~29% of conversion efficiency directly from the OPA.

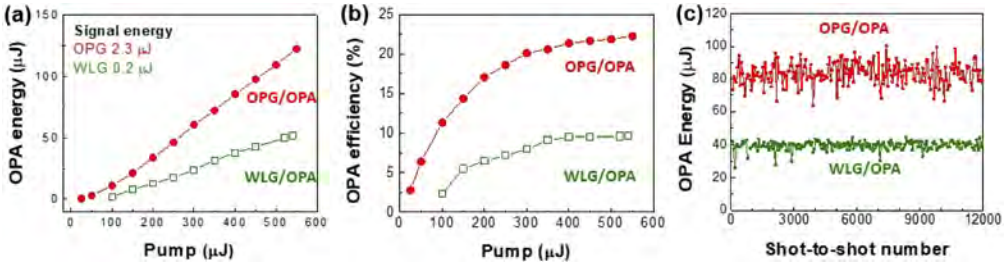

Fig. 5. Generated beam performance through ZGP OPA: (a) Output OPA pulse energies vs. pump energy, (b) conversion efficiency vs. pump energy, and (c) shot-to-shot energy stabilities.

The pulse energy stability is important for reliable applications of OPA output pulses. Figure 5(c) shows the shot-to-shot energy stability of signal and idler combined pulses, measured with the 3 μm LPF to block unconverted pump energy. Here, we set the output pulse energy to 40 μJ and 80 μJ from the WLG/OPA and OPG/OPA, respectively, and measured the shot-to-shot rms stability over 12,000 shots. With the 2.4 μm pump laser stability of ~4.6% rms, we observed some degradation to ~6.6% rms with WLG/OPA and ~8.2% rms with OPG/OPA. In fact, since the energy stability of the Cr:ZnSe pump laser can be enhanced to ~2.5% rms (the latter half of Fig. 1(c)) with re-optimization along the sufficient warm-up time, the OPA stability can be enhanced to ~3 – 5% level as well. Regarding the long-term energy stability, no noticeable degradation was observed over many hours. The OPG/OPA was less stable than the WLG/OPA because OPG is based on a spontaneous amplification progress starting from a noise, but it can be further improved if we use a longer ZGP crystal for OPG to saturate the gain.

For the temporal characterization of amplified signal pulses, we used a home-built intensity autocorrelator with a 2-mm-thick polycrystalline ZnSe window as a second-harmonic generation (SHG) and sum-frequency generation (SFG) medium based on random quasi-phase matching (RQPM) [27] that supports ultrabroad phase matching in the mid-IR. The SHG and SFG of the signal pulse in the range of 1.5-2.4 μm were detected using the near-IR spectrometer. Figure 6(a) illustrates the setup of the autocorrelator for the ultrabroadband mid-IR pulses. A 300-μm-thick Si plate was used as a BS at 45° angle of incidence. With a delay stage and a metallic off-axis parabolic mirror (OAP), two beams are temporally overlapped at and focused into the ZnSe window for SFG in a noncollinear geometry. We tuned the input pulse energy such that it is just high enough for SHG from each arm and then maximized the SFG (AC signal) with the delay scan while cutting out the background SHG from each arm using a slit. Figures 6(b) and (c) show the measured AC trace of the pulses from WLG/OPA and OPG/OPA, exhibiting an AC width of 466 and 450 fs in FWHM, respectively. The corresponding pulse duration is 330 and 318 fs, respectively, with the Gaussian assumption of temporal profile. Both cases show the minor pulse broadening from the pump pulse duration (~250 fs) indicating the minimal GVM between pump and signal (~10 fs/mm from Fig. 2(c)).

Given the broad spectral bandwidth of the signal beam (~1000 nm in FWHM), the signal pulses can be compressed to the few-optical-cycle range (<30 fs) for WLG/OPA. The idler pulse duration was not measured in this work, but it is also expected to be close to the pump duration with the minimal GVM (<10 fs/mm over 5 – 10 μm from Fig. 2(c)) for both WLG/OPA and OPG/OPA. The idler pulses from WLG/OPA can be compressed to the sub-two-cycle range given the octave-spanning spectral bandwidth. While the compressibility of OPG/OPA pulses needs to

Optics EXPRESS

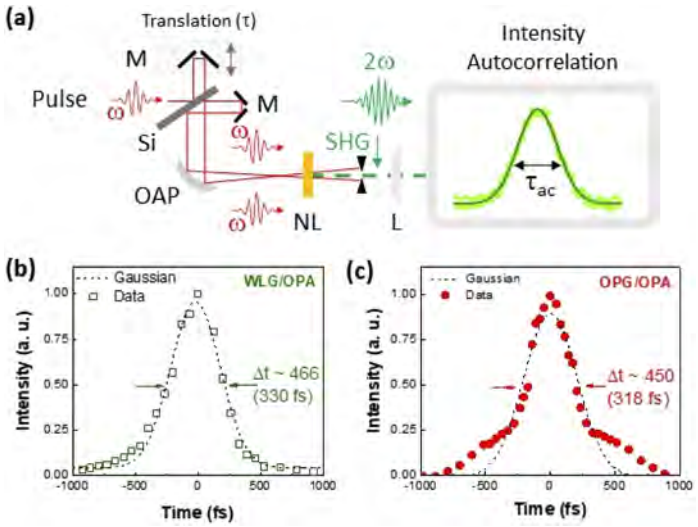

Fig. 6. (a) Scheme of the intensity autocorrelator. M, Al mirror; OAP, off-axis parabolic mirror; NL, 2 mm-thick polycrystalline ZnSe. The measured AC trace of the signal pulse from WLG/OPA (b) and OPG/OPA (c) along with Gaussian fitting.

be further investigated, the femtosecond pulse duration of signal beam indicates that the spectral phase is at least partially coherent over the ultrabroad spectral band.

3.3.3. Spectrally filtered OPA

The mid-IR OPA output can be re-optimized for relatively narrowband operation with spectral tunability for specific applications. In this work, we attempted to maximize the OPG/OPA spectrum at 4.15 μm to seed a Fe:ZnSe amplifier operating at the 3.5 – 4.5 μm range [28]. For the spectral filtering we used a BPF at 4.15 μm in ~200 nm bandwidth with 70% of transmittance after the OPG stage and then re-optimized the spatial and temporal overlaps between the pump and seed beams. The OPA output was filtered again with a 4.2 μm BPF in ~420 nm bandwidth to remove any residual SF outside the desired spectral band. The resultant spectrum is shown in Fig. 7, where the pulse energy of ~30 μJ was obtained (0.55 mJ of pump) in the spectral bandwidth of 200 nm. The inset of Fig. 7 confirms a good near-field output beam profile. While

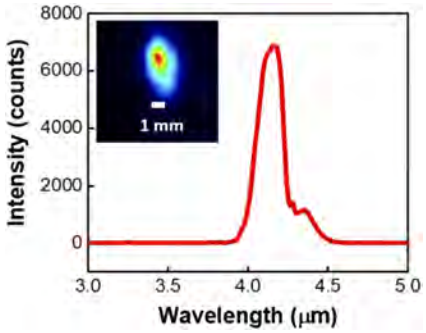

Fig. 7. The spectrally filtered and re-optimized spectrum centered at 4.15 μm with 30 μJ output energy obtained from OPG/OPA. The inset shows the near-field beam profile of the amplified signal.

Optics EXPRESS

the conversion efficiency can be further increased with a longer ZGP crystal, the pulse energy with the spectrum in Fig. 7 is high enough to seed a ultrafast Fe:ZnSe amplifier for multi-mJ ~4 μm pulse generation [28].

4. Conclusions

We successfully developed a highly-efficient, robust mid-IR femtosecond OPA system with ZGP that fully covers the wavelength range from 3 to 10 μm, pumped by a 2.4 μm Cr:ZnSe laser operating at a 1 kHz repetition rate. A systematic and comparative study of WLG-seeded OPA and OPG-seeded OPA was presented. The maximum output energy of 130 μJ and the conversion efficiency of 23% were obtained from the OPG-seeded OPA scheme thanks to the high seed energy (~2.3 μJ), while the moderate pulse energy (55 μJ) and efficiency (10%) were obtained with the WLG-seeded OPA. To the best of our knowledge, our OPG-seeded OPA is the most efficient mid-IR OPA source generating a greater-than-octave-spanning spectrum. The energy scalability is guaranteed with additional OPA stages given that high-power mid-IR pump lasers and high-quality large-area ZGP crystals are available. In addition, we demonstrated relatively narrowband OPA at ~4.15 μm for seeding a Fe:ZnSe amplifier.

At the demonstrated energy level, ultrashort mid-IR laser pulses are already attractive for applications such as spectroscopic chemical detections, high-order harmonic generation in solids, laser filamentation in solids, and dielectric laser acceleration in nano-structures.

Funding

MIT Lincoln Laboratory (ACC program, IR10-773); National Institute of Environmental Health Sciences (P42 ES027723); Office of Naval Research (DURIP, N00014-17-1-2744); U.S. Department of Energy (DE-SC0018378).

Acknowledgement

Drs. E. P. Ippen (MIT) and F. X. Kärtner (CFEL-DESY, Germany) are appreciated for the general support with the laboratory infrastructure at MIT. Drs. S. Vasilyev and J. Peppers (IPG Photonics SETC) are appreciated for design and installation of the Cr:ZnSe regenerative amplifier at MIT.

Disclosures

The MIT authors declare no conflicts of interest. The work reported here partially involves intellectual property developed at the UAB. This intellectual property has been licensed to the IPG Photonics Corporation. Drs. Fedorov and Mirov declare competing financial interests.

This material is based upon work supported by the United States Air Force under Air Force Contract No. FA8702-15-D-0001. Any opinions, findings, conclusions or recommendations expressed in this material are those of the author(s) and do not necessarily reflect the views of the United States Air Force.

References

1. A. J. Fleisher, B. J. Bjork, T. Q. Bui, K. C. Cossel, M. Okumura, and J. Ye, "Mid-Infrared Time-Resolved Frequency Comb Spectroscopy of Transient Free Radicals," J. Phys. Chem. Lett. **5**(13), 2241–2246 (2014).
2. M. Wagner, A. S. McLeod, S. J. Maddox, Z. Fei, M. Liu, R. D. Averitt, M. M. Fogler, S. R. Bank, F. Keilmann, and D. N. Basov, "Ultrafast Dynamics of Surface Plasmons in InAs by Time-Resolved Infrared Nanospectroscopy," Nano Lett. **14**(8), 4529–4534 (2014).
3. J. Weisshaupt, V. Juvé, M. Holtz, S. Ku, M. Woerner, T. Elsaesser, S. Ališauskas, A. Pugžlys, and A. Baltuška, "High-brightness table-top hard X-ray source driven by sub-100-femtosecond mid-infrared pulses," Nat. Photonics **8**(12), 927–930 (2014).
4. S. Wandel, M.-W. Lin, Y. Yin, G. Xu, and I. Jovanovic, "Parametric generation and characterization of femtosecond mid-infrared pulses in $ZnGeP_2$," Opt. Express **24**(5), 5287–5299 (2016).

Optics EXPRESS

5. D. Sanchez, M. Hemmer, M. Baudisch, S. L. Cousin, K. Zawilski, P. Schunemann, O. Chalus, C. Simon-Boisson, and J. Biegert, "7 μm, ultrafast, sub-millijoule-level mid-infrared optical parametric chirped pulse amplifier pumped at 2 μm," Optica **3**(2), 147–150 (2016).
6. H. Liang, P. Krogen, Z. Wang, H. Park, T. Kroh, K. Zawilski, P. Schunemann, J. Moses, L. F. DiMauro, F. X. Kärtner, and K.-H. Hong, "High-energy mid-infrared sub-cycle pulse synthesis from a parametric amplifier," Nat. Commun. **8**(1), 141 (2017).
7. K. Liu, H. Liang, L. Wang, S. Qu, T. Lang, H. Li, Q. J. Wang, and Y. Zhang, "Multi-microjoule GaSe-based midinfrared optical parametric amplifier with an ultrabroad idler spectrum covering 4.2–16 μm," Opt. Lett. **44**(4), 1003–1006 (2019).
8. P. Malevich, T. Kanai, H. Hoogland, R. Holzwarth, A. Baltuška, and A. Pugžlys, "Broadband mid-infrared pulses from potassium titanyl arsenate/zinc germanium phosphate optical parametric amplifier pumped by Tm,Ho-fiber-seeded Ho:YAG chirped-pulse amplifier," Opt. Lett. **41**(5), 930 (2016).
9. S. B. Mirov, V. V. Fedorov, I. S. Moskalev, D. Martyshkin, and C. Kim, "Progress in Cr^{2+} and Fe^{2+} Doped Mid-IR Laser Materials," Laser Photonics Rev. **4**(1), 21–41 (2010).
10. S. B. Mirov, S. Vasiyev, V. Smolski, V. V. Fedorov, D. Martyshkin, J. Peppers, M. Mirov, A. Degachev, and V. Gapontsev, "Frontiers of mid-IR lasers based on transition metal doped chalcogenides," IEEE J. Sel. Top. Quantum Electron. **24**(5), 1–29 (2018).
11. S. B. Mirov, V. V. Fedorov, D. Martyshkin, I. S. Moskalev, M. Mirov, and S. Vasilyev, "Progress in mid-IR lasers based on Cr and Fe-doped II-VI chalcogenides," IEEE J. Sel. Top. Quantum Electron. **21**(1), 292–310 (2015).
12. S. Vasilyev, I. Moskalev, M. Mirov, S. Mirov, and V. Gapontsev, "Multi-Watt mid-IR femtosecond polycrystalline Cr^{2+}:ZnS and Cr^{2+}:ZnSe laser amplifiers with the spectrum spanning 2.0–2.6 μm," Opt. Express **24**(2), 1616–1623 (2016).
13. S. Vasiliev, I. Moskalev, M. Mirov, V. Smolski, S. Mirov, and V. Gapontsev, "Ultrafast middle-IR lasers and amplifiers based on polycrystalline Cr:ZnS and Cr:ZnSe," Opt. Mater. Express **7**(7), 2636–2650 (2017).
14. S. Vasilyev, I. S. Moskalev, V. O. Smolski, J. M. Peppers, M. Mirov, A. V. Muraviev, K. Zawilski, P. G. Schunemann, S. B. Mirov, K. L. Vodopyanov, and V. P. Gapontsev, "Super-octave longwave mid-infrared coherent transients produced by optical rectification of few-cycle 2.5-μm pulses," Optica **6**(1), 111–114 (2019).
15. N. Nagl, S. Gröbmeyer, V. Pervak, F. Krausz, O. Pronin, and K. F. Mak, "Directly diode-pumped, Kerr-lens mode-locked, few-cycle Cr:ZnSe oscillator," Opt. Express **27**(17), 24445–24454 (2019).
16. P. Komm, U. Sheintop, S. Noach, and G. Marcus, "Carrier-to-envelope phase-stable, mid-infrared, ultrashort pulses from a hybrid parametric generator: Cr:ZnSe laser amplifier system," Opt. Express **27**(13), 18522–18532 (2019).
17. X. Ren, L. H. Mach, Y. Yin, Y. Wang, and Z. Chang, "Generation of 1 kHz, 2.3 mJ, 88 fs, 2.5 μm pulses from a Cr^{2+}:ZnSe chirped pulse amplifier," Opt. Lett. **43**(14), 3381–3384 (2018).
18. S. Vasilyev, J. Peppers, I. Moskalev, V. Smolski, M. Mirov, E. Slobodchikov, A. Dergachev, S. Mirov, and V. Gapontsev, "1.5-mJ Cr:ZnSe Chirped Pulse Amplifier Seeded by a Kerr-Lens Mode-Locked Cr:ZnS oscillator," *Laser Congress 2019 (ASSL, LAC, LS&C), OSA Technical Digest* (Optical Society of America, 2019), paper ATu4A.4
19. S.-H. Nam, G. C. Nagar, D. Dempsey, O. Novak, B. Shim, and K.-H. Hong, "Resonant Radiation of Mid-infrared Laser Filaments Driven by a 2.4 μm Femtosecond Cr:ZnSe Laser," *Frontiers in Optics and Laser Science 2019* (OSA, Washington D.C.), JW4A.111.
20. A. V. Smith, SNLO, public-domain software (AS-Photonics). It is available as a free download at http://www.as-photonics.com/snlo
21. D. E. Zelmon, E. A. Hanning, and P. G. Schunemann, "Refractive-index measurements and Sellmeier coefficients for zinc germanium phosphide from 2 to 9 μm with implications for phase matching in optical frequency-conversion devices," J. Opt. Soc. Am. B **18**(9), 1307–1310 (2001).
22. K.-H. Hong, C.-J. Lai, J. Siqueira, P. Krogen, J. Moses, C.-L. Chang, G. J. Stein, L. E. Zapata, and F. X. Kärtner, "Multi-mJ, kHz, 2.1-μm optical parametric chirped pulse amplifier and high-flux soft X-ray high-harmonic generation," Opt. Lett. **39**(11), 3145–3148 (2014).
23. A. Dergachev, "High-energy, kHz-rate, picosecond, 2-μm laser pump source for mid-IR nonlinear optical devices," Proc. SPIE **8599**, 85990B (2013).
24. S. Wandel, G. Xu, Y. Yin, and I. Jovanovic, "Parametric generation of energetic short mid-infrared pulses for dielectric laser acceleration," J. Phys. B: At., Mol. Opt. Phys. **47**(23), 234016 (2014).
25. C. Manzoni and G. Cerullo, "Design criteria for ultrafast optical parametric amplifiers," J. Opt. **18**(10), 103501 (2016).
26. F. Silva, D. R. Austin, A. Thai, M. Baudisch, M. Hemmer, D. Faccio, A. Couairon, and J. Biegert, "Multi-octave supercontinuum generation from mid-infrared filamentation in a bulk crystal," Nat. Commun. **3**(1), 807 (2012).
27. M. Baudrier-Raybaut, R. Haïdar, P. Kupecek, P. Lemasson, and E. Rosencher, "Random quasi-phase-matching in bulk polycrystalline isotropic nonlinear materials," Nature **432**(7015), 374–376 (2004).
28. E. Migal, A. Pushkin, B. Bravy, V. Gordienko, N. Minaev, A. Sirotkin, and F. Potemkin, "2.5-mJ 150-fs Fe:ZnSe hybrid mid-IR femtosecond laser at 4.4 μm for driving extreme nonlinear optics," Opt. Lett. **44**(10), 2550–2553 (2019).